



The 10m-resolution global leaf chlorophyll content product using Sentinel-2 based on chlorophyll sensitive index CSI

Hu Zhang¹, Jing Li^{1,2}, Chenpeng Gu^{2,3}, Li Guan^{1,2}, Xiaohan Wang^{2,3}, Faisal Mumtaz^{2,3}, Yadong Dong¹, Jing Zhao¹, Qinhua Liu^{2,3}, Shangrong Lin⁴, Wentao Yu⁵

5 ¹ Key Laboratory of Remote Sensing and Digital Earth, Aerospace Information Research Institute, Chinese Academy of Sciences, Beijing 100101, China

² University of Chinese Academy of Sciences, Beijing 100049, China

³ National Engineering Research Center for Satellite Remote Sensing Applications, Chinese Academy of Sciences, Beijing 100101, China

10 ⁴ Carbon-Water Research Station in Karst Regions of Northern Guangdong, School of Geography and Planning, Sun Yat-Sen University, Guangzhou 510006, China

⁵ Center for Geospatial Information, Shenzhen Institute of Advanced Technology, Chinese Academy of Science, Shenzhen 518055, China

15 *Correspondence to:* Jing Li (lijing200531@aircas.ac.cn); Qinhua Liu (liuqh@aircas.ac.cn)

Abstract. Leaf chlorophyll content (LCC) is an essential biochemical parameter reflecting vegetation's photosynthetic activity. In the past five years, some global LCC remote sensing products have been generated, and play an important role in vegetation growth monitoring and terrestrial carbon cycle modeling. However, the resolution of current global LCC products ranges from 300m to 500m, and the existing 30m-resolution product, Multi-source data Synergized Quantitative remote sensing production system LCC (MuSyQ LCC), is only available in China, resulting in a lack of global high-resolution LCC products. This study used an empirical relationship method based on the chlorophyll sensitive index (CSI) to produce a 10m resolution global LCC product (MuSyQ Global LCC) with the Google Earth Engine (GEE) platform. A web application was developed, allowing users to independently select regions of interest, time ranges, and spatial-temporal resolutions. The validation results show the MuSyQ Global LCC consists well with the current global MODIS LCC, and MuSyQ Global LCC's (RMSE = 14.16 $\mu\text{g}/\text{cm}^2$, bias = 1.68 $\mu\text{g}/\text{cm}^2$) accuracy is slightly higher than that of MODIS LCC (RMSE = 14.74 $\mu\text{g}/\text{cm}^2$, bias = -2.65 $\mu\text{g}/\text{cm}^2$). The 10m-resolution LCC product has an RMSE of 15.33 $\mu\text{g}/\text{cm}^2$, R^2 of 0.27, and the accuracy of the vegetation types-specific regression model is stable in different sites across the world. The high-resolution LCC product can show more details of spatial distribution and reasonable temporal profiles than the existing low-resolution product, indicating its ability in precision agriculture, forestry monitoring, and related research.

30 1 Introduction

Chlorophyll is an essential pigment in green plants' photosynthesis that harvests solar radiation and absorbs carbon dioxide. Leaf chlorophyll content (LCC) indicates the maximum carboxylation rate (V_{cmax}) (Lu et al., 2022) and can then be used to



calculate the primary productivity of plants (Gitelson et al., 2003). LCC also indicates light, temperature, water stress, pests, and diseases. Therefore, the accurate large-scale LCC can improve the performance of the terrestrial global carbon cycle model (Luo et al., 2018, 2019) and the ability of ecosystem monitoring. Remote sensing methods, taking advantage of chlorophyll's varied absorption and scattering properties in different bands, make it the only applicable approach to retrieve LCC at the continental or global scale.

In the past decades, some progress has been made in LCC inversion algorithms, which can be classified into two categories. One category is the radiometric transfer model (RTM) based method. PROSPECT + SAIL (PROSAIL) model (Jacquemoud et al., 2009), SCOPE model (van der Tol et al., 2009), and 4-Scale model (Chen and Leblanc, 1997) are widely used RTMs in leaf pigment estimation (Botha et al., 2007; Feret et al., 2008; Singh et al., 2023; Xu et al., 2019). Based on the two models, look-up-table (LUT) or machine learning methods are usually employed for the LCC calculation. Due to the precise physical mechanisms of the model, the RTM-based model is generalizable when applied to vegetation of different types or in different areas. Another is the empirical VI-based method. Due to its high efficiency and convenience, many VIs sensitive to chlorophyll content have been developed to estimate it (Croft et al. 2014) at the regional or global scale. It is easy to produce a reasonable LCC result. Still, many chlorophyll indices are always compounded by the information of canopy and background, such as leaf area index (LAI), leaf angle distribution (LAD), and soil brightness (Ref). Zhang et al. (2022) proposed an LCC-sensitive-and-LAI-insensitive chlorophyll-sensitive index (CSI), which is highly sensitive to the LCC but insensitive to the LAI and soil reflectance. It has applicability to estimate the global scale LCC using sensors with edge sensors such as Sentinel-2 and Gaofen-6 (Gu et al., 2023).

Some global LCC products are generated using RTM-based or empirical VI-based methods. MERIS LCC product is the first global LCC whose spatial resolution is 300m and temporal resolution is 7 days (Croft et al., 2020). Leaf-level radiative transfer model PROSPECT combined with the 4-Scale model (for woody vegetation) and SAIL model (for non-woody vegetation) were used to construct LUTs to derive LCC from the MERIS data. The validation result suggested the product achieved an R^2 of 0.47 and an RMSE of $10.79 \mu\text{g}/\text{cm}^2$. MODIS LCC is the product generated by MODIS data from a VI matrix method (Xu et al., 2022a). The spatial resolution is 500m, and the temporal resolution is 8 days. The product shows a good agreement with Landsat-up scaled LCC ($R^2 = 0.77$ and $\text{RMSE} = 6.9 \mu\text{g}/\text{cm}^2$) from ground measurements. GLCC products were derived from ENVISAT MERIS and Sentinel-3 OLCI with a spatial resolution of 500m and a temporal resolution of 7 days (Qian et al., 2023). LUTs constructed from the PROSPECT-D + 4-Scale model (for heterogeneous vegetation) and PROSPECT-D + 4SAIL model (for homogenous vegetation) were used to derive global LCC. Another global LCC product is the GLOBMAP MERIS LCC (Xu et al., 2022b). Based on the RTM simulations, a neural network was constructed and derived from the ENVISAT MERIS LCC with a resolution of 300m/7 days from 2003 to 2012. The RMSE and R^2 of the product are $9.7 \mu\text{g}/\text{cm}^2$ and 0.54. The current global LCC product's spatial resolution is from 300m to 500m. A recent study compared the performance of these LCC products in China and showed that the RMSE ranged from $21.0 \mu\text{g}/\text{cm}^2$ to $32.3 \mu\text{g}/\text{cm}^2$ (Wang et al., 2024), indicating the accuracy still requires systematic improvement. In the scale of 300 - 500m, a large proportion of vegetation areas should be in the mixed pixels (Yu et al., 2018), and the mixed-pixel effect brings great uncertainties to the inversion of vegetation



parameters (Yang et al., 2014). Enhancing the spatial resolution becomes a practical way to improve the accuracy of the current product. Meanwhile, the higher-resolution product is a more effective reference for decision-making in fine precision agriculture and grazing and a more reasonable input of global and regional ecosystem models associated with carbon cycle modeling (Schimel et al., 2015).

The only published large-scale and high-resolution LCC product is the Multi-source data Synergized Quantitative remote sensing production system LCC (MuSyQ LCC, (Guan et al., 2025; Li et al., 2021)). Using Sentinel-2 MSI reflectance and CSI-based empirical regression method, the resolution of the LCC product was improved to 30m/10 days. The product's root mean squared error (RMSE) is 9.39 $\mu\text{g}/\text{cm}^2$ in different vegetation types, and the accuracy is relatively stable in different LAI and LCC conditions. Wang et al., (2024) compare the MuSyQ LCC product with the other lower-resolution. Results suggest the MuSyQ LCC has the highest accuracy, demonstrates high overall spatial consistency, and highly correlates with the MODIS LCC over China. Additionally, the MuSyQ product is constrained by the revisit period of Sentinel-2, resulting in data gaps during the 10-day composite period, with a missing rate ranging around 20% - 50%. However, when the composite period is adjusted to a month, the missing data problem is greatly eliminated. Therefore, its algorithm is stable and suitable for generating the large-scale LCC product. However, the MuSyQ LCC product only covers China from 2019 to 2020 without high-resolution global LCC information.

This study aims to 1) generate the first high-resolution global LCC product (MuSyQ Global LCC) by using the CSI-based method; 2) develop a web application that allows users to generate and download their customized LCC products of their regions of interest (ROIs), the time ranges, the spatial and temporal resolutions (<https://code.earthengine.google.com/a06dfc261ad8019e025153d5bd0e68ca>); 3) validate the generated MuSyQ global LCC product using the ground-measured LCC in different sites across the world, and compare its accuracy with the existing MODIS LCC.

2 Data and Methods

2.1 Satellite data

Sentinel-2 Multispectral Instrument (MSI) images generated the MuSyQ Global LCC product. The European Space Agency (ESA) Sentinel-2 Earth observation mission consists of two satellites, Sentinel-2A, and Sentinel-2B, with a revisit frequency of 5 days in equatorial regions. The MSI onboard Sentinel-2 has 13 bands including three red-edge bands sensitive to the LCC. The spatial resolution of Sentinel-2 is 10 m for visible and near-infrared (NIR) bands and 20 m for the red-edge bands. The Sentinel-2 MSI level 2 (L2A) land surface reflectance product, pre-processed with radiometric calibration geometric and atmospheric correction, is an ideal dataset for calculating the CSI index and retrieving the LCC. The Sentinel-2 MSI L2A dataset is available on both the official website (<https://dataspace.copernicus.eu/>) and the Google Earth Engine (GEE) platform. In this study, we processed the Sentinel-2 MSI L2A dataset in 2019-2022 on the GEE platform to calculate LCC, and the calculated LCC is resampled to a specific resolution using the nearest neighbor method.



2.2 Land cover data

The product of Global Land Cover with a Fine Classification System at 30 m (Zhang et al., 2021) was used to define the vegetation types. Based on the GLC_FCS30 land-cover product, vegetation worldwide was reclassified into five major types: broadleaf forest, needleleaf forest, cropland, grassland, and shrub. Empirical regression relationships between LCC and CSI were constructed for each type.

2.3 Ground measurements

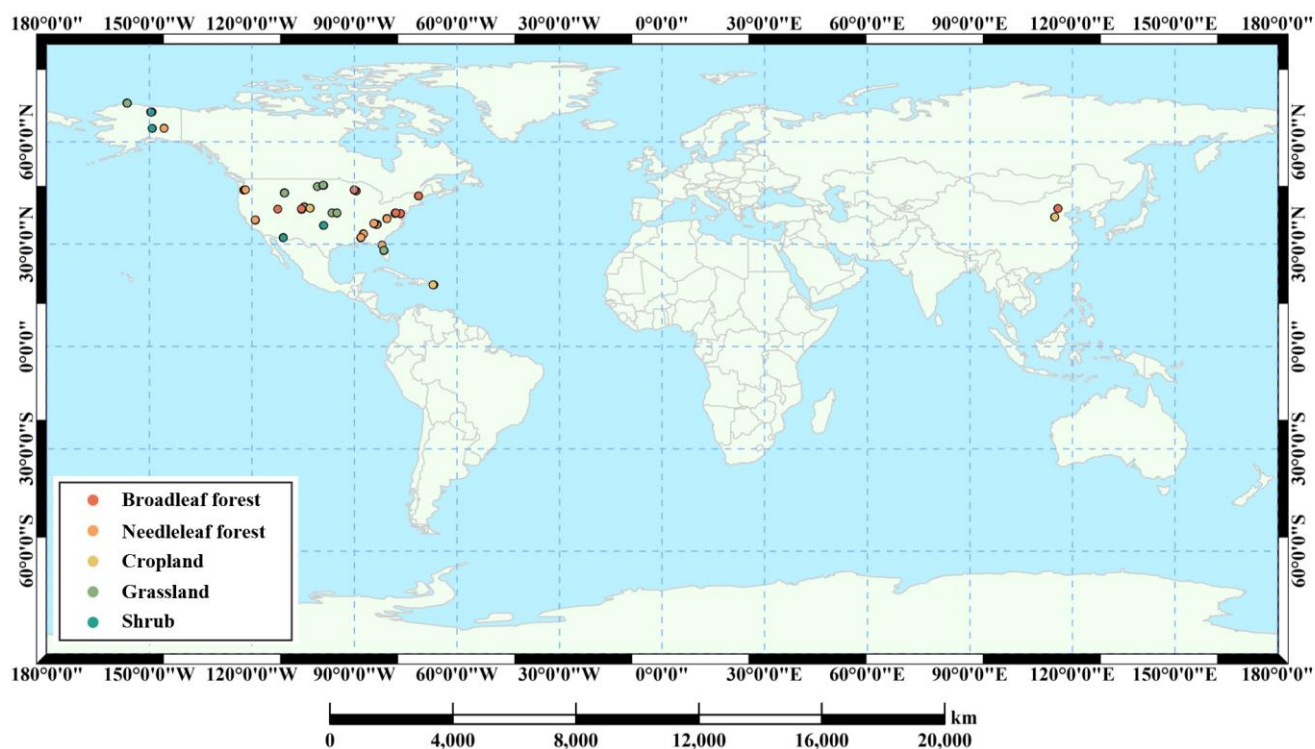
The ground-measured LCC from different research is collected to validate the MuSyQ Global LCC product. Table 2 and Figure 1 show the details of the experiments and the spatial distribution of the ground-measured LCC data. These data encompassed 1199 sampling measurements in different field campaigns, including the National Ecological Observatory Network (NEON) in the USA, Huailai and Gaocheng field experiments in China. The least size of each experiment is 20m * 20m, which can validate the product with 10m spatial resolution. As for the validation of the 100m-resolution and the 500m-resolution LCC products, the ground-measured LCC should be filtered first because experiments were designed for the high-resolution LCC validation, and the plots are only kept homogenous in the scale of 20m (Gaocheng), 30m (Huailai), and 40m scale (NEON). The 30m-resolution land cover product (GLC_FCS30) was used to assess if plots in Huailai and NEON are located in a homogenous area. The centre coordinates of each plot in the experiment and its vegetation type in GLC_FCS30 were extracted. For the validation of the 100m resolution product, sampling points are selected based on the presence of data with the same GLC_FCS30 product value within a 5*5 pixel area (i.e., 150m x 150m homogeneous). For the validation of the 500m resolution product, sampling points are chosen within a 17*17 pixel area that shares the same GLC_FCS30 product value (i.e., 510m x 510m homogeneous).

Table 1 Ground measurements of LCC used for the validation of 30m-resolution LCC.

Vegetation Type	Number of Samplings	Value Range ($\mu\text{g}/\text{cm}^2$)	Sampling Year	LCC Dataset	Reference
Broadleaf Forest	419	3.74 – 78.86	2020, 2021, 2022, 2023	NEON (USA) Huailai (China)	(National Ecological Observatory Network (NEON), 2024; Zhang et al., 2022)
Needleleaf Forest	335	7.29 – 78.63	2020, 2021, 2022, 2023	NEON (USA) Huailai (China)	(National Ecological Observatory Network (NEON), 2024; Zhang et al., 2022)
Cropland	165	3.22 – 81.09	2020, 2021, 2022, 2024	NEON (USA) Huailai (China) Gaocheng (China)	(National Ecological Observatory Network (NEON), 2024; Zhang et al., 2022)



Grassland	225	10.98 – 80.61	2016, 2020, 2021, 2022, 2023	NEON (USA) Huailai (China)	(National Ecological Observatory Network (NEON), 2024; Zhang et al., 2022)
Shrub	55	17.06 – 76.23	2020, 2021, 2022, 2023	NEON (USA)	(National Ecological Observatory Network (NEON), 2024)



120

Figure 1: Spatial distribution of the ground-measured LCC.

2.3.1 National Ecological Observatory Network (NEON) LCC dataset

The LCC dataset across the USA was obtained from the freely accessible NEON, an ecological observation platform including multiple ecological sites (<https://data.neonscience.org/data-products/DP1.10026.001>). In this study, 374 broadleaf forest measurements, 303 needleleaf forest measurements, 71 cropland measurements, 182 grassland measurements, and 55 shrub measurements in 2020-2023 are collected for validation.

2.3.2 Huailai LCC dataset

The time of LCC experiments in Huailai covers the winter of 2020 to the summer of 2021. Homogenous plots of 30 m × 30 m for different vegetation types are selected for the Chl_{leaf} measurements. Plants in different locations of each plot were selected

130



and leaves at three different heights (top, middle, and bottom) of the selected plants were harvested and transported to the laboratory. Foliar chlorophyll was extracted with 25 ml ethanol with a volume fraction of 80%, and the concentration of chlorophyll a ($Chla_i$) and b ($Chlb_i$) in the unit of mg/ml was calculated based on the absorbance recorded at wavelengths of 663 nm and 646 nm (α_{663} , α_{646}) using a Lambda 25 spectrophotometer (PerkinElmer Inc., USA) as equation (1) and (2).

$$Chla_i \text{ (mg/ml)} = 12.21 * \alpha_{663} - 2.81 * \alpha_{646} \quad (1)$$

$$Chlb_i \text{ (mg/ml)} = 20.13 * \alpha_{646} - 5.03 * \alpha_{663} \quad (2)$$

$Chla_i$ and $Chlb_i$ can be converted to the LCC_i by equation (3).

$$LCC_i \text{ (}\mu\text{g/cm}^2\text{)} = (Chla_i + Chlb_i) * 25 / A_i \quad (3)$$

This dataset includes 45 broadleaf forest measurements, 32 needleleaf forest measurements, 29 cropland measurements, and 43 grassland measurements.

2.3.3 Gaocheng LCC dataset

The Gaocheng cropland LCC experiment was conducted on April 12 and April 25, 2024. There are 65 homogenous winter wheat plots of 20 m \times 20 m. The hand-held chlorophyll meter (SPAD-502, Minolta Osaka Company Ltd., Tokyo, Japan) was used to measure the SPAD values of the wheat leaves in different locations within each plot. After each field measurement, some leaves in the site were randomly collected and then transported to the laboratory to calibrate the model between SPAD and LCC. SPAD values were read and then the LCC was measured using the Lambda 25 spectrophotometer, using the same method as the Huailai experiment. The calibration regression models between SPAD and LCC for April 12, 2024 (equation 4) and April 25, 2024 (equation 5) are shown as follows.

$$LCC \text{ (}\mu\text{g/cm}^2\text{)} = 1.1339 * SPAD - 5.5071 \quad (4)$$

$$LCC \text{ (}\mu\text{g/cm}^2\text{)} = 3.3983 * SPAD - 112.95 \quad (5)$$

2.4 Method to generate the MuSyQ Global LCC

Figure 2 illustrates the diagram to generate the high-resolution LCC product. Firstly, the Sentinel-2 MSI L2A product is selected to calculate CSI, and the global vegetation cover map derived from the GLC_FCS30D product is reclassified into five types. Then, using the type-specific regression equations (Table 2), LCC for different vegetation is calculated on the GEE platform. A cloud score based on the Sentinel-2 MSI is calculated to evaluate the cloud possibility and the cloud-contaminated pixels can be identified using the algorithm (https://github.com/openforis/gee-gateway/blob/master/gee_gateway/gee_utils.py#L691). Subsequently, to make the max value of the product 80 $\mu\text{g/cm}^2$, any value larger than 80 $\mu\text{g/cm}^2$ is set to 80 $\mu\text{g/cm}^2$. In this way, the 1-day LCC with the same resolution with Sentinel-2 MSI is generated. Next, several 1-day LCC maps of the same tiles are averaged and resampled to produce the customized LCC product with different spatial and temporal resolutions. Finally, the generated MuSyQ Global LCC is compared with the existing 500m-resolution MODIS LCC product and validated using the ground-measured LCC.



165 The large volume of global high-resolution product data requires substantial storage space, and uploading such data can be
 extremely time-consuming. More importantly, defining regions of interest and changing resolutions based on users' needs is
 not feasible. Therefore, we only uploaded the global 100m/10 days resolution LCC product in 2019-2013 to the online server
 and provided a web interface based on the GEE platform, allowing users to independently select their desired temporal and
 spatial ranges as well as the corresponding resolutions
 170 (<https://code.earthengine.google.com/a06dfc261ad8019e025153d5bd0e68ca>). The instructions for the web interface can be
 seen in the User Manual in the Supplement.

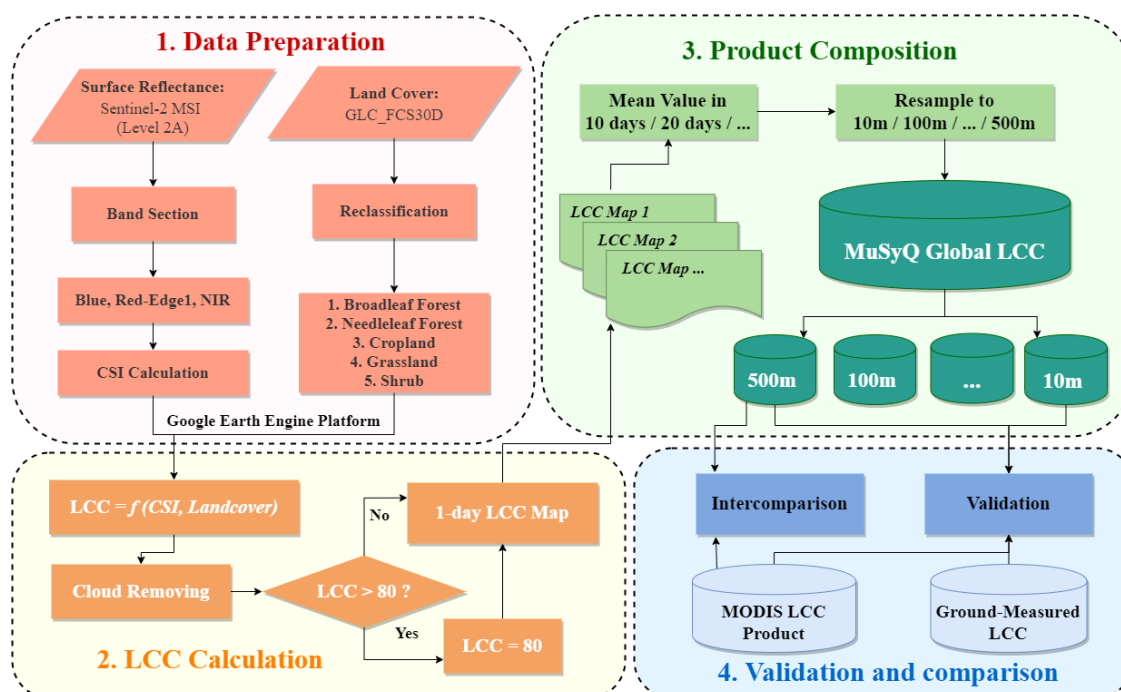


Figure 2: Diagram of generating the LCC product

175 Table 2 Empirical regression equation between CSI and LCC in different vegetation types. The regression equations were derived using PROSAIL simulation.

Vegetation Type	Equations	RMSE ($\mu\text{g}/\text{cm}^2$)	R ²
Broadleaf Forest	$LCC = 99.31 * CSI - 9.78$	6.04	0.93
Needleleaf Forest	$LCC = 121.99 * CSI - 15.97$	6.18	0.93
Cropland	$LCC = 76.92 * CSI + 2.00$	7.70	0.68
Grassland	$LCC = 89.18 * CSI + 0.03$	6.61	0.99
Shrub	$LCC = 130.34 * CSI - 25.37$	10.21	0.88



2.5 Assessment of the LCC product

The performance metrics of the LCC product include the root mean squared error (RMSE), relative RMSE (rRMSE), the coefficient of determination (R^2), and the averaged bias (bias). They are defined as follows. RMSE, rRMSE, and R^2 are accuracy indicators showing the discrepancy between the LCC product and the ground-measured LCC (LCC_{true}).

$$RMSE = \sqrt{\frac{1}{n} \sum_{i=1}^n [LCC_{product}(i) - LCC_{true}(i)]^2} \quad (6)$$

$$rRMSE = RMSE / \overline{LCC_{true}} \quad (7)$$

$$R^2 = \frac{\sum_{i=1}^n [LCC_{product}(i) - \overline{LCC_{true}}]^2}{\sum_{i=1}^n (LCC_{true}(i) - \overline{LCC_{true}})^2} \quad (8)$$

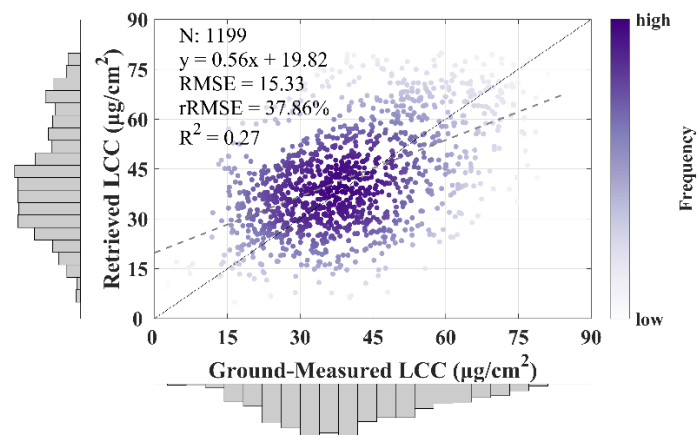
Bias was selected in this study to show the algorithm's overestimation or underestimation.

$$Bias = \frac{1}{N} \sum_{i=1}^n [LCC_{product}(i) - LCC_{true}(i)] \quad (9)$$

3 Results

3.1 Validation of 10m-resolution MuSyQ Global LCC product with ground measurements

Figure 3 illustrates the validation result of the 10m-resolution MuSyQ Global LCC product. The results suggest the overall RMSE and rRMSE of the product in 5 different vegetation types were $15.33 \mu\text{g}/\text{cm}^2$, 37.86%, respectively, and the R^2 was 0.27. The LCC retrieved from the 10m-resolution product and the ground-measured LCC were aligned along the 1:1 line, with underestimation under high LCC conditions and overestimation under low LCC conditions. Figure 4 shows the detailed results in different vegetation types. The accuracy of the retrieved LCC is varied with an RMSE between 11.44 and $20.21 \mu\text{g}/\text{cm}^2$ in the five types. The cropland had the highest accuracy with an RMSE of $11.44 \mu\text{g}/\text{cm}^2$, rRMSE of 19.71%, and bias of $1.30 \mu\text{g}/\text{cm}^2$. The grassland had the accuracy with an RMSE of $12.01 \mu\text{g}/\text{cm}^2$, rRMSE of 35.52%, and bias of $1.41 \mu\text{g}/\text{cm}^2$. The RMSE, rRMSE, and bias of broadleaf forest were higher, with $15.60 \mu\text{g}/\text{cm}^2$, 39.64, and $4.70 \mu\text{g}/\text{cm}^2$, respectively. LCC of needle leaf forest and the shrub had the lowest accuracy, with RMSE of $17.57 \mu\text{g}/\text{cm}^2$ and $20.21 \mu\text{g}/\text{cm}^2$. Figure 4 also shows LCC product for all five types tended to be underestimated when LCC is more than $60 \mu\text{g}/\text{cm}^2$ and the LCC was overestimated for forests, grasslands, and shrubs when LCC is less than $30 \mu\text{g}/\text{cm}^2$.



200 **Figure 3: Validation of the 10m-resolution MuSyQ Global LCC**

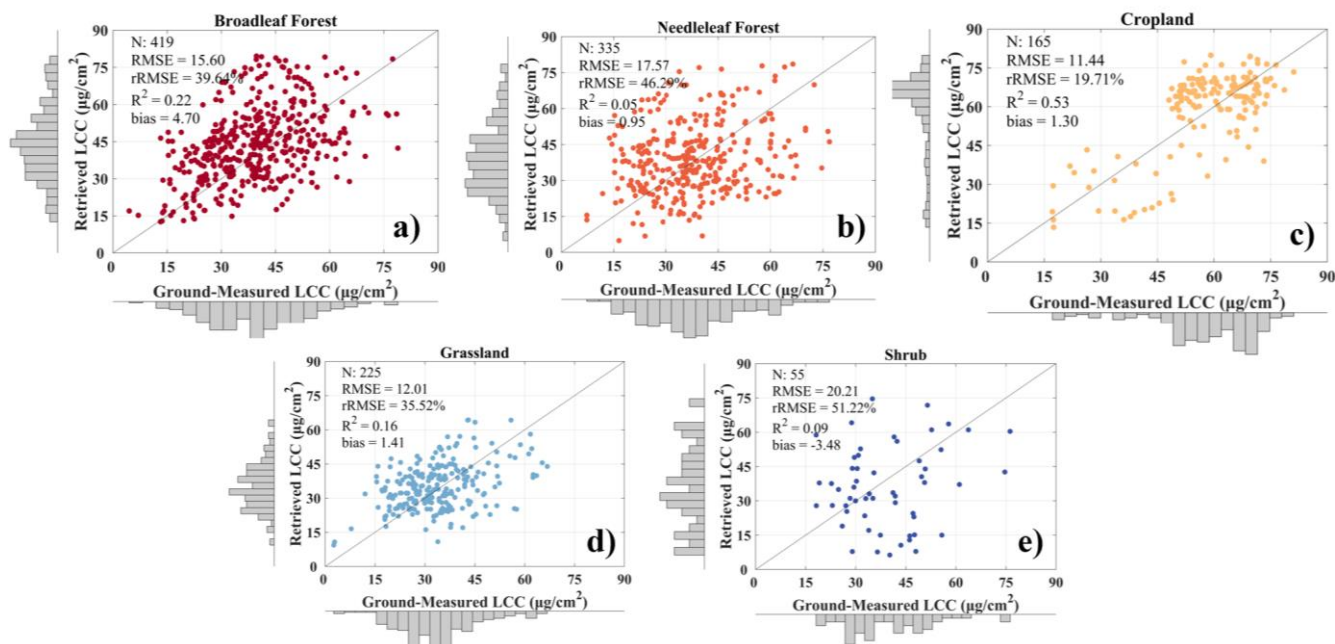


Figure 4: Validation results of the 10m-resolution MuSyQ Global LCC in different vegetation types

Figure 5 shows the product's bias under different LCC conditions. Due to the limited number of ground-measured LCCs of shrubs, only the other four types were compared. Generally, the LCC retrieved from the product tended to be overestimated
 205 when the LCC was less than $20 \mu\text{g}/\text{cm}^2$. The bias of broadleaf forest, needleleaf forest, and grassland was more than $10 \mu\text{g}/\text{cm}^2$. When the LCC was $20 - 40 \mu\text{g}/\text{cm}^2$, the overestimation became less obvious, especially for the cropland, whose bias is close to $0 \mu\text{g}/\text{cm}^2$. When LCC increased, the overestimation gradually turned to underestimation for the broadleaf, needleleaf, and grassland. When the ground-measured LCC was $60 - 80 \mu\text{g}/\text{cm}^2$, the bias of the product for broadleaf forest and grassland



declined to below $15 \mu\text{g}/\text{cm}^2$. As for the bias of cropland, it fluctuated with the increase in LCC. Apart from the condition of
 210 LCC = $40 - 60 \mu\text{g}/\text{cm}^2$, the mean bias of the product is close to $0 \mu\text{g}/\text{cm}^2$, indicating the overestimation or underestimation is
 relatively slight.

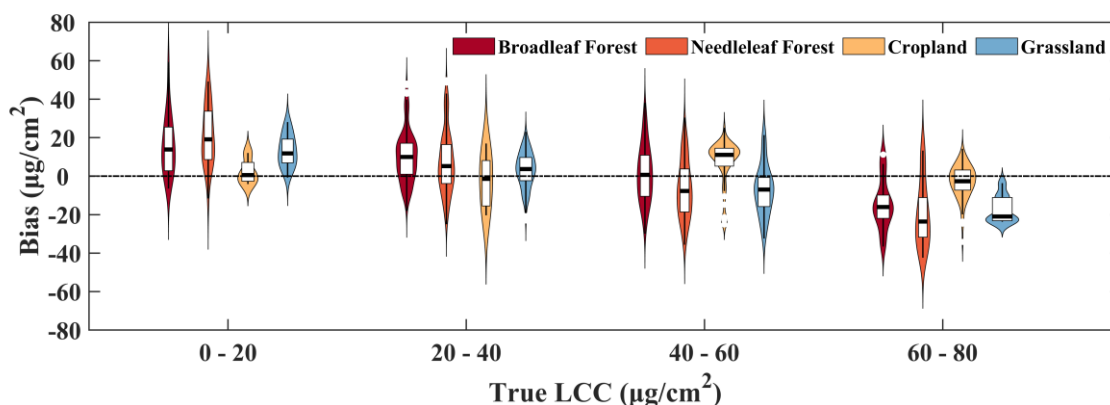


Figure 5: Bias of the LCC product under different LCC conditions. Due to the limited number of shrubs, only the first four vegetation types are compared. The black line within each violin represents the mean value of the bias and the box represents the value of the upper and lower quartiles.
 215

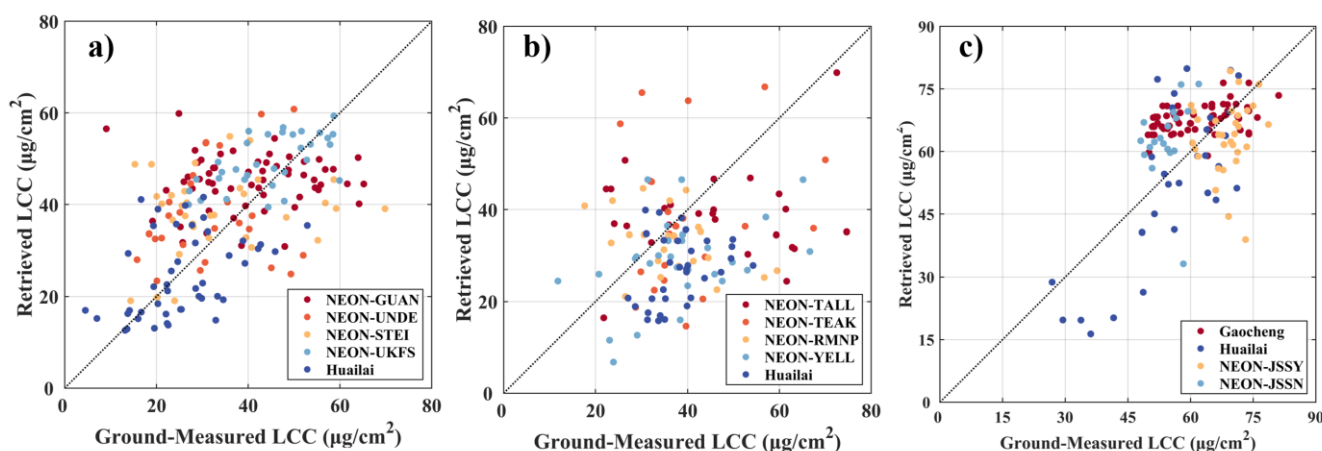
To evaluate if the LCC calculated algorithm is stable in different regions, the accuracy of the LCC product in different sampling sites is compared. Table 3 illustrates each site's location, the RMSE, and the bias of the LCC product, and Figure 6 shows the scattering plots of the site-specific and type-specific validation results. Five sites with large variations of the latitude in the USA ($17.9706^\circ\text{N} - 46.2359^\circ\text{N}$) and one site in China are selected for the broadleaf forest. In all sites, although the LCC varied
 220 with sites from less than $5 \mu\text{g}/\text{cm}^2$ to more than $70 \mu\text{g}/\text{cm}^2$, the RMSE of the LCC product was very stable with the range of $9.15 - 15.57 \mu\text{g}/\text{cm}^2$. The bias was between $-1.05 \mu\text{g}/\text{cm}^2$ and $6.05 \mu\text{g}/\text{cm}^2$, meaning the LCC algorithm showed no severe overestimation or underestimation across the broadleaf sites. For the LCC in the sites of needleleaf forest, although the error was larger than that of broadleaf forest and underestimation existed when LCC was high, the RMSE within this vegetation type was also stable. The RMSE was from 14.09 to $18.63 \mu\text{g}/\text{cm}^2$. The four sites of the cropland across China and the USA
 225 also had similar RMSE, ranging from 9.63 to $12.97 \mu\text{g}/\text{cm}^2$ and the variation of the bias was from $-5.24 \mu\text{g}/\text{cm}^2$ to $8.76 \mu\text{g}/\text{cm}^2$.

Table 3 Location of each site and the accuracy of the MuSyQ Global LCC product in each site

Vegetation Type	Site Name	Latitude	Longitude	RMSE	Bias
a) Broadleaf Forest	NEON-GUAN	17.9706°N	66.8627°W	12.96	3.43
	NEON-UNDE	46.2359°N	89.5337°W	14.46	6.05
	NEON-STEI	45.7019°N	89.8998°W	15.57	4.74
	NEON-UKFS	39.0425°N	95.1938°W	9.15	4.91
	Huailai	40.3594°N	115.7999°E	10.24	-1.05
b) Needleleaf Forest	NEON-TALL	32.9353°N	87.4157°W	18.63	-5.63



	NEON-TEAK	37.0009°N	119.0283°W	18.12	-2.67
	NEON-RMNP	40.1953°N	105.5154°W	14.52	-3.62
	NEON-YELL	44.9531°N	110.4980°W	15.28	-9.51
	Huailai	40.3484°N	115.7841°E	14.09	-11.50
	Gaocheng	37.8814°N	114.8552°E	9.63	6.23
c) Cropland	Huailai	40.3470°N	115.7802°E	12.97	-2.98
	NEON-JSSY	33.9126°N	120.3411°W	10.62	-5.24
	NEON-JSSN	33.9874°N	117.8651°W	12.66	8.76



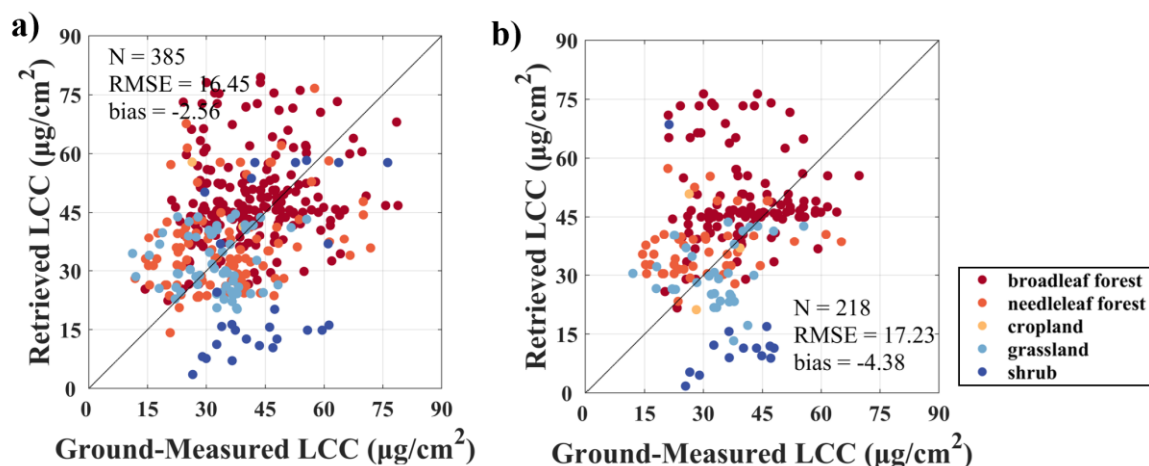
230

Figure 6: Accuracy of the MuSyQ Global LCC product in different vegetation types and different sites.

3.2 Accuracy of the MuSyQ Global LCC Product at the Hectometer Scale

The published 100m-resolution MuSyQ Global LCC product (link:xxxx) was validated using the 385 ground measurements (Figure 7a and Table 4). The accuracy (RMSE = 16.45 $\mu\text{g}/\text{cm}^2$, bias = -2.56 $\mu\text{g}/\text{cm}^2$, $R^2 = 0.11$) was lower than the 10m-resolution product for all five vegetation types. The grassland had the highest accuracy with the RMSE, and bias of 11.19 $\mu\text{g}/\text{cm}^2$, and -0.19 $\mu\text{g}/\text{cm}^2$. The shrub had a relatively low RMSE and bias of 25.60 $\mu\text{g}/\text{cm}^2$ and -2.64 $\mu\text{g}/\text{cm}^2$, respectively. The accuracy of the shrub was relatively low. The RMSE was 25.60 $\mu\text{g}/\text{cm}^2$, and the underestimation was severe with a value of -18.37 $\mu\text{g}/\text{cm}^2$. For the 500m-resolution product, which shares the same resolution as the MODIS LCC product, its overall accuracy was lower than that of the 100m-resolution product, meaning that the resolution is an important factor contributing to the accuracy of the LCC product. RMSE rose to 17.23 $\mu\text{g}/\text{cm}^2$ and the overall bias was -4.38 $\mu\text{g}/\text{cm}^2$. The overestimation of the broadleaf forest, the needleleaf forest, and the underestimation of shrubs became more significant when the resolution decreased.

240



245 **Figure 7: Validation of the 100m-resolution a) and the 500m-resolution MuSyQ Global LCC product b) in different vegetation types**

Table 4 Accuracy of 100m-resolution LCC product in different vegetation types

	100m			500m		
	N	RMSE ($\mu\text{g}/\text{cm}^2$)	Bias ($\mu\text{g}/\text{cm}^2$)	N	RMSE ($\mu\text{g}/\text{cm}^2$)	Bias ($\mu\text{g}/\text{cm}^2$)
Broadleaf Forest	195	16.83	6.79	122	17.52	8.44
Needleleaf Forest	92	15.26	1.42	45	14.23	7.10
Cropland	2	22.32	16.79	2	14.77	5.06
Grassland	62	11.19	-0.19	34	11.25	-2.31
Shrub	27	25.60	-18.37	14	30.99	-23.29
All Types	385	16.45	2.56	218	17.23	-4.38

Due to the temporal overlap of MODIS LCC product (2000 - 2020) and available Sentinel-2 imagery (L2A level, after 2019) on the GEE platform being limited to 2019 and 2020, the study selected validation points from these two years for an intercomparison between the products (Figure 8). There were 57 validation points, including where the two 500m products overlapped from 2019 to 2020. The validation data included three vegetation types (broadleaf forest, needleleaf forest, and grassland in Table 5). In the validation of these 57 points, the accuracy of the two products was similar, with the MuSyQ LCC product showing slightly higher accuracy than the MODIS LCC product. The RMSE and bias improved from 14.74 $\mu\text{g}/\text{cm}^2$ and -2.65 $\mu\text{g}/\text{cm}^2$ to 14.16 $\mu\text{g}/\text{cm}^2$ and 1.68 $\mu\text{g}/\text{cm}^2$, respectively. In the 500m scale, the two products tended to show an obvious underestimation under high LCC conditions. The MuSyQ Global LCC product exhibited lower RMSE for broadleaf forests and grasslands. In comparison, the RMSE for needleleaf forests was higher than that of the MODIS product (Table 5).

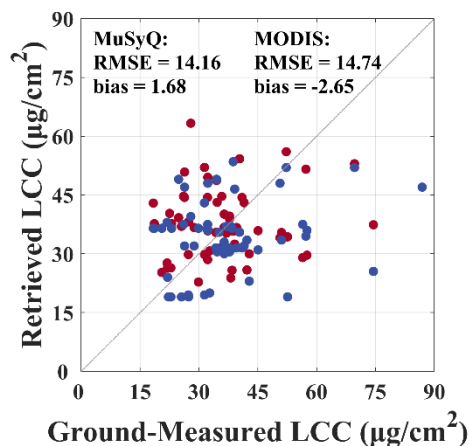


Figure 8: Validation of the 500m-resolution MuSyQ Global LCC product and 500m-resolution MODIS LCC

Table 5 Accuracy of MuSyQ Global LCC and MODIS LCC product in different vegetation types

	MuSyQ Global LCC (500m)			MODIS LCC		
	N	RMSE (µg/cm ²)	Bias (µg/cm ²)	N	RMSE (µg/cm ²)	Bias (µg/cm ²)
Broadleaf Forest	9	14.80	5.65	9	20.69	0.34
Needleleaf Forest	22	13.96	6.11	22	10.26	2.97
Grassland	26	14.12	-3.28	26	15.46	-8.44
All Types	57	14.16	1.68	57	14.74	-2.65

260

3.3 Comparison of spatial distributions between MuSyQ Global LCC and MODIS LCC

Figure 9 illustrates the global distribution of the MuSyQ LCC product in January and July 2020. The line chart on the right illustrates the variation in average LCC across different latitudes. Overall, global LCC was lower in January compared to July. In the region between 0-30°S, LCC was relatively high, with an average close to 40 µg/cm². The highest LCC values were observed in the mid to low-latitude regions of eastern South America and Africa. Additionally, the low-latitude areas of the northern hemisphere, such as the Indian subcontinent, also exhibited high LCC values. In the other northern hemisphere regions, LCC was generally below 30 µg/cm² due to the winter season. In July, the average LCC in the 30°N - 60°N region was above 20 µg/cm², and in the 45°N - 75°N region, it was generally above 30 µg/cm². The map showed that the highest LCC values were found in the northern parts of the Eurasian continent and the mid-latitude eastern regions of North America. In contrast, the Southern Hemisphere generally exhibited lower LCC values, mostly below 20 µg/cm².

270

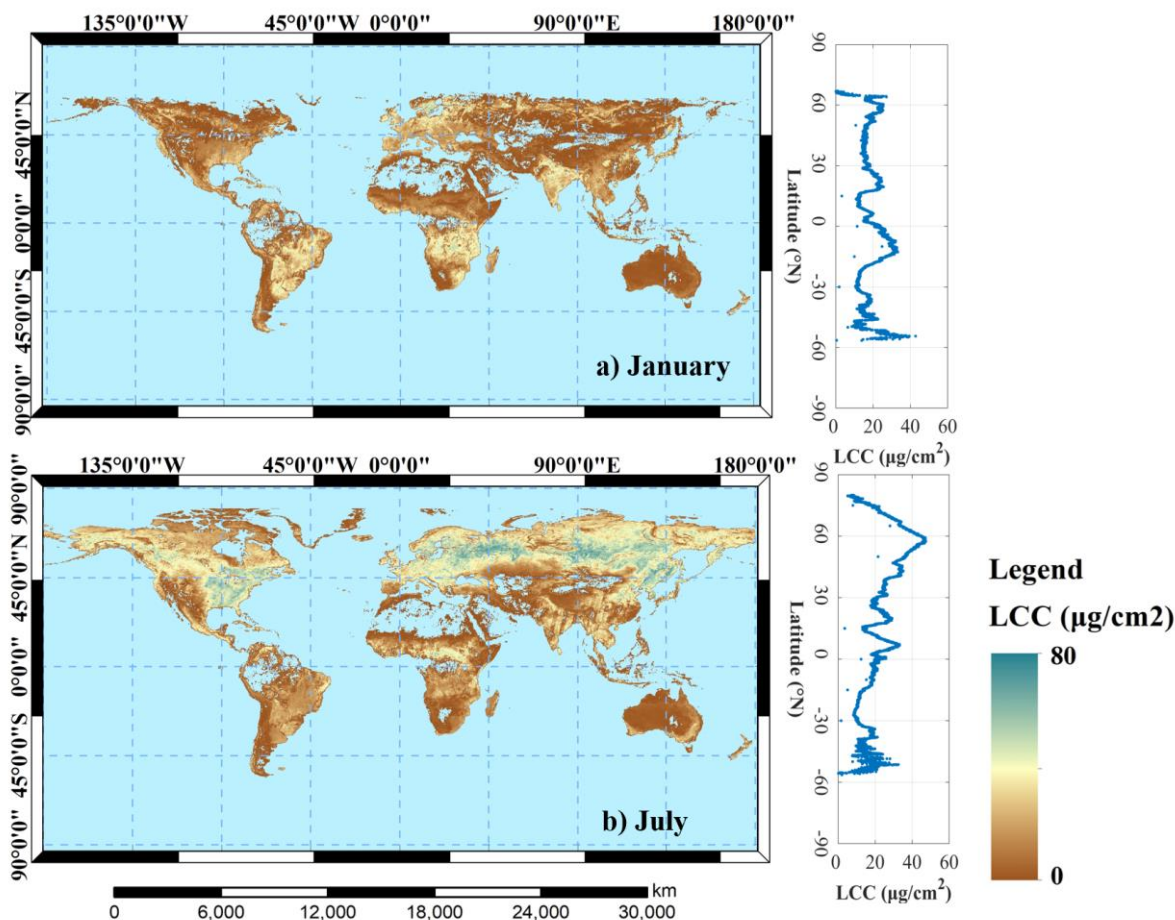


Figure 9: Global distribution of the MuSyQ Global LCC product. The product was resampled to 1km, and the mean values of the LCC products in January 2020 (a) and July 2020 (b) were included in the map. The line chart represented the averaged LCC in different latitudes.

275 Figure 10 illustrates the differences between the January and July MuSyQ Global LCC and MODIS LCC products. In January, the MuSyQ Global LCC product was generally lower than the MODIS product in the southern hemisphere, while in the mid to high-latitude regions of the northern hemisphere, the MuSyQ Global LCC was slightly higher than the MODIS LCC. The histogram on the right showed that the distribution of Δ LCC was more concentrated in the negative value region, indicating that the values of the MuSyQ Global LCC in January were lower than those of the MODIS LCC. Additionally, the Δ LCC for most pixels was within $\pm 5 \mu\text{g}/\text{cm}^2$, suggesting good consistency between the two products. Figure 10b shows the spatial distribution of the differences between the two products during the summer. The regions with the largest Δ LCC were in the northeastern part of the Eurasian continent, northeastern North America, southern Africa, and the eastern regions of the southern hemisphere. The regions with the smallest Δ LCC were in the western part of the Eurasian continent, the Northern Hemisphere regions of Africa, and western Australia. The histogram on the right indicated that in July, the peak of Δ LCC was

280



285 around $0 \mu\text{g}/\text{cm}^2$, and the distribution of the histogram was more symmetrical compared to January, with no significant
tendency towards the negative value region.

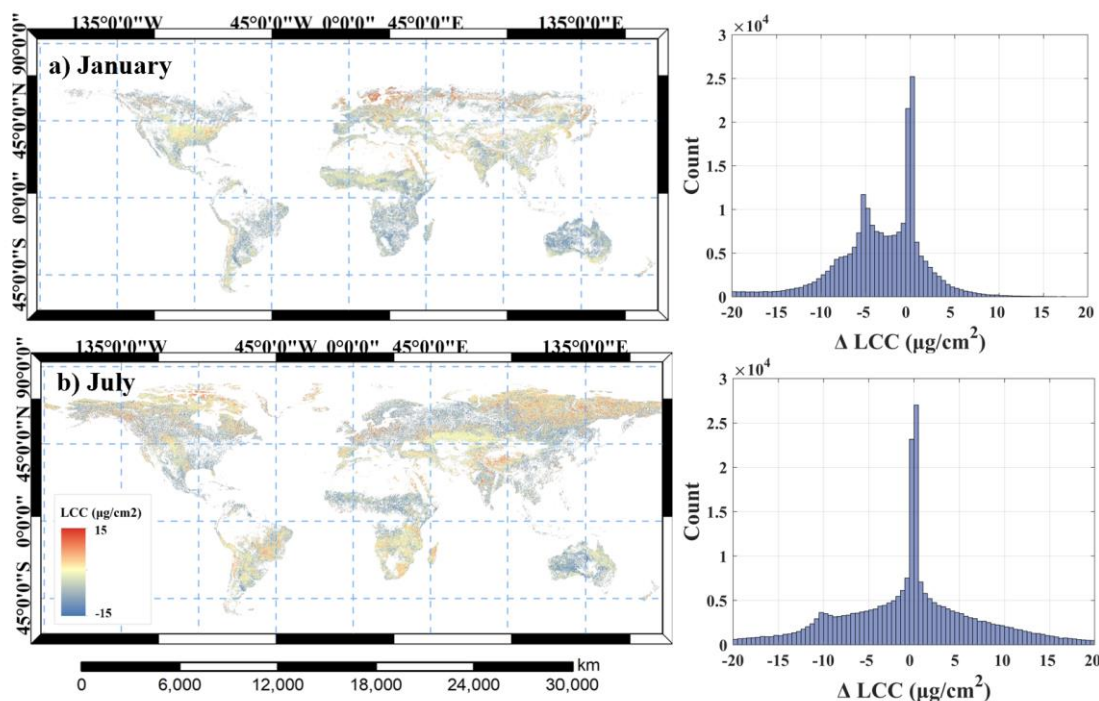


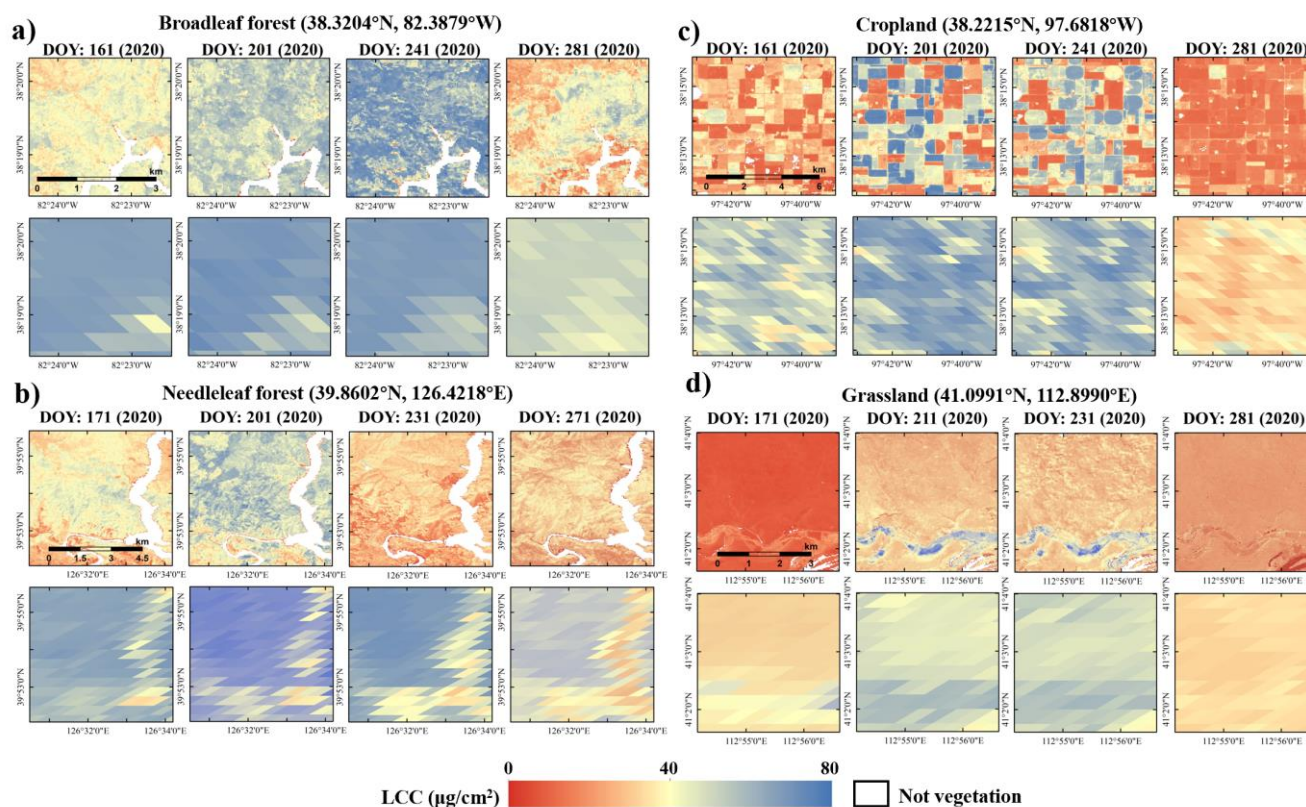
Figure 10: Difference between MuSyQ Global LCC and MODIS LCC in January and July 2020. $\Delta\text{LCC} = \text{MuSyQ Global LCC} - \text{MODIS LCC}$.

290

Figure 12 compares the spatial details of the two products in regions of different vegetation types. The spatial resolution of MuSyQ Global LCC was set to 10m, while the spatial resolution of MODIS LCC was 500m. Figure 12a, b shows the 10m-resolution MuSyQ Global LCC product clearly illustrated the spatial distribution of the forests' LCC, with the zero-value areas along the southeastern river being distinctly identifiable. However, in the 500m-resolution MODIS LCC product, forests were represented by a few averaged values with small differences, and the river only contributes to an overall slightly lower pixel value, with no obvious spatial distribution. As shown in Figure 12c, the 10-meter resolution MuSyQ Global LCC product revealed the differences in LCC among various agricultural fields during the summer (DOY = 201, 241). The distinct boundaries between different plots in the 10 m resolution LCC product could be easily identified. In contrast, due to its low spatial resolution, the MODIS LCC product failed to show the boundaries between fields, with pixel values only reflecting the overall conditions within a 500-meter-scale area. For the relatively homogeneous grasslands, the spatial distribution characteristics of the two products showed smaller differences. However, the MuSyQ Global LCC product exhibited a lower tendency than the MODIS LCC product and could capture more spatial distribution details of LCC during the summer (DOY 211, 231 in Figure 12d).

295

300

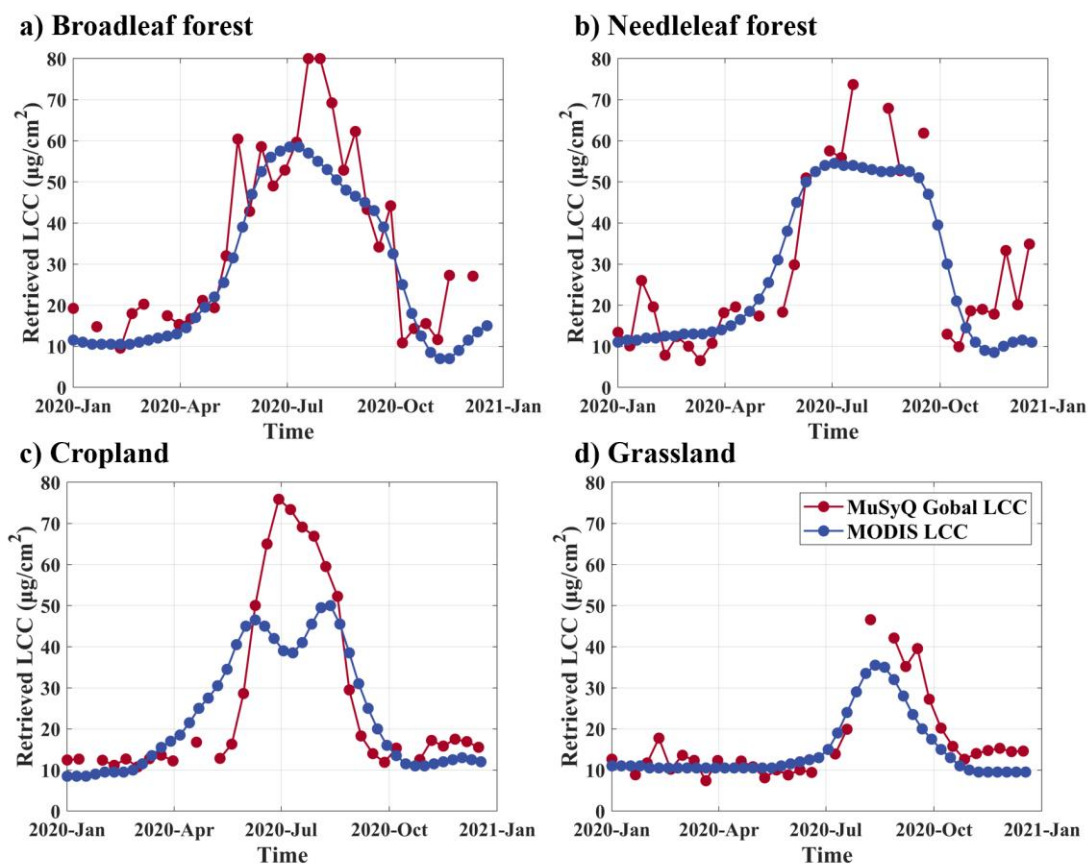


305 **Figure 11: Spatial details of LCC in broadleaf forest a), needleleaf forest b), cropland c) and grassland d) areas**

3.4 Comparison of temporal profiles between MuSyQ Global LCC and MODIS LCC

Figure 12 compares the temporal profiles of the four specific vegetation types in Figure 12. Both products effectively captured the phenological characteristics of typical vegetation types, showing an initial increase followed by a decrease in LCC. The MuSyQ Global LCC product generally fluctuated between adjacent time points, while the MODIS LCC time series curve was smooth. Additionally, the 10m-resolution MuSyQ Global LCC showed higher values than the 500m-resolution MODIS LCC for all four types during the summer, which is the primary difference between the two products. For broadleaf forests, coniferous forests, and crops, the MuSyQ Global LCC reached values above $70 \mu\text{g}/\text{cm}^2$ during the summer, while the maximum values of the MODIS LCC were all below $60 \mu\text{g}/\text{cm}^2$. For grasslands, the maximum value of the MuSyQ Global LCC approached $50 \mu\text{g}/\text{cm}^2$, whereas the MODIS LCC was below $40 \mu\text{g}/\text{cm}^2$.

310



315

Figure 12: Temporal profile of four typical vegetation types in Figure 11.

4 Discussion

4.1 Advantages of the high-resolution LCC product

320 Existing global-scale LCC products have spatial resolutions of 300m or 500m. Although 30m-resolution LCC products have been published, their temporal coverage is limited to 2019 and 2020, and their spatial extent is restricted to China (<https://doi.org/10.11922/sciencedb.j00001.00265>). This study generates the first global high-resolution LCC product (MuSyQ Global LCC), which can be acquired using the published web interface (link: <https://code.earthengine.google.com/a06dfc261ad8019e025153d5bd0e68ca>). For the 100m-resolution product, it is now available online (see the link in Section 5).

325 MuSyQ Global LCC shows a reasonable spatial distribution of global LCC (Figure 9). It demonstrates good consistency with existing MODIS LCC products in a 500m scale (Figure 8), with over 85% of the pixel differences between the two products remaining within $\pm 5 \mu\text{g}/\text{cm}^2$ in January and July (Figure 10). However, unlike the MODIS LCC products, the MuSyQ Global



LCC product generated in this study can achieve a resolution of 10m. This enhanced resolution allows for the easy capture of spatial distribution differences in LCC within agricultural areas (Figure 11c), attributed to variations in crop varieties, planting
330 times, and management practices, demonstrating its potential application in crop phenotyping. In forested areas as shown in Figure 11a, b, the high-resolution LCC product can also reflect spatial differences in LCC, which will benefit forestry monitoring and management.

On a global scale, the proportion of pure pixels in vegetated areas at a 1km resolution is only 35% (Yu et al., 2018). The heterogeneity within the pixels is a significant factor limiting the accuracy of existing low-resolution products. A recent study
335 compared different LCC products and showed that the RMSE of these products ranged from 19.5 $\mu\text{g}/\text{cm}^2$ to 32.3 $\mu\text{g}/\text{cm}^2$ and increasing the resolution significantly enhances the accuracy of the products (Wang et al., 2024). Figure 3 and Figure 7 demonstrate that the RMSEs of the product were 17.23 $\mu\text{g}/\text{cm}^2$, 16.45 $\mu\text{g}/\text{cm}^2$, and 15.33 $\mu\text{g}/\text{cm}^2$ when the spatial resolution of the output product was set to 500m, 100m, and 10m. All accuracies in these three different resolutions are higher than products
340 compared in the study of (Wang et al., 2024), which means the high accuracy provided by high-resolution data sources will enable the high-resolution MuSyQ Global LCC product to play a more significant role in ecosystem monitoring. Even after being resampled to a 500m resolution, its accuracy was higher than that of the MODIS LCC with RMSE of 14.16 $\mu\text{g}/\text{cm}^2$ and 14.74 $\mu\text{g}/\text{cm}^2$ (Figure 8).

The MuSyQ Global LCC product was generated using the CSI-based empirical regression algorithm, and the regression model may vary between sites because it is easily affected by factors such as LAI, LAD, soil reflectance, etc. According to previous
345 studies, the CSI maintains high sensitivity to LCC, while remaining insensitive to factors such as LAI, LAD, and soil background (Gu et al., 2023; Zhang et al., 2022). This characteristic allows for the production of global products with a high level of accuracy using the general regression models in Table 2 across the global scale. As shown in Figure 6 and Table 3, the product accuracy for each vegetation type across different global sites showed a small variation. In the broadleaf forest sites, the RMSE was from 9.15 $\mu\text{g}/\text{cm}^2$ to 15.57 $\mu\text{g}/\text{cm}^2$ across four NEON sites distributed throughout the United States, while
350 the RMSE for the Huailai site in China was 10.24 $\mu\text{g}/\text{cm}^2$. In the needleleaf forest sites, the RMSE for the NEON sites in the United States ranged from 14.52 $\mu\text{g}/\text{cm}^2$ to 18.63 $\mu\text{g}/\text{cm}^2$, with the Huailai site in China showing an RMSE of 14.09 $\mu\text{g}/\text{cm}^2$, and all exhibiting varying degrees of underestimation. For the crop sites, the RMSE for the Huailai and Gaocheng sites in China ranged from 9.63 $\mu\text{g}/\text{cm}^2$ to 12.97 $\mu\text{g}/\text{cm}^2$, while the RMSE for the two NEON sites in the United States was between 10.62 $\mu\text{g}/\text{cm}^2$ and 12.66 $\mu\text{g}/\text{cm}^2$. These results indicated no significant accuracy differences between countries and sites,
355 suggesting generality in the regression equations for each vegetation type.

4.2 Uncertainties of the high-resolution global LCC product

High-resolution satellites typically have limited swath widths, resulting in longer revisit periods. The revisit period of Sentinel-2 is 5 days; issues such as cloud and rain cover can lead to pixel missing in the 10-day composite product. The validation
360 results of the MuSyQ product for China in 2019 indicated that the retrieval rate for the 10-day composite products varies



between 50% and 80% throughout different periods of the year, with the data missing being more severe in winter compared to summer (Wang et al., 2024). If the composite period were extended to one month, the data missing would be significantly reduced (Figure 9). In the future, the reconstruction algorithm of the time series for the LCC will further enhance the applicability of the MuSyQ Global LCC product.

365 The MuSyQ Global LCC product utilizes the blue band, which is sensitive to atmospheric aerosols. Consequently, variations in atmospheric conditions during Sentinel-2 imaging can lead to fluctuations in LCC values, resulting in uneven brightness patterns, as illustrated in Figure 9b for the South Asia region. Additionally, for the high-resolution products, errors in the cloud masking algorithm can result in high LCC values at the edges of cloud shadows that are sometimes difficult to eliminate, leading to overestimating cloud shadows. More accurate atmospheric correction and cloud masking algorithms will further
370 enhance the accuracy of this product.

The validation dataset in this study is mainly in China and the United States, with limited availability of ground measurements from other countries or regions. As a result, the validation results may not represent the accuracy on a global scale. Additionally, differences in LCC measurement methods and sampling strategies across various sites may introduce errors when the validation set is applied to different scales. A larger and more comprehensive ground-measured LCC dataset will be beneficial
375 for assessing the accuracy of LCC products.

5 Data availability

The MuSyQ Global LCC product with 100m/10 days in the year 2019-2023 can be accessed at Science Data Bank (Table 6).

Table 6 DOI of the MuSyQ Global Leaf Chlorophyll Content product with 100m/10 days resolution

Assets Name	DOI	Reference
MuSyQ Global LCC product (2019)	https://doi.org/10.57760/sciencedb.19595	(Zhang et al., 2025a)
MuSyQ Global LCC product (2020)	https://doi.org/10.57760/sciencedb.19687	(Zhang et al., 2025b)
MuSyQ Global LCC product (2021)	https://doi.org/10.57760/sciencedb.19689	(Zhang et al., 2025c)
MuSyQ Global LCC product (2022)	https://doi.org/10.57760/sciencedb.19691	(Zhang et al., 2025d)
MuSyQ Global LCC product (2023)	https://doi.org/10.57760/sciencedb.19692	(Zhang et al., 2025e)

380

The web application was developed that allows users to generate their customized LCC products of their regions of interest (ROIs), time ranges, the spatial and temporal resolutions. This GEE APP allows users to draw the LCC temporal profile of the selected pixel without login (<https://ee-425490093.projects.earthengine.app/view/lcc-gee-app>). If the users want to download LCC images for their region of interest, the following link can be used, <https://code.earthengine.google.com/a06dfc261ad8019e025153d5bd0e68ca>, but logging into their GEE account is mandatory, as these images will be automatically
385 transferred to their Google Drive. For detailed instructions, please refer to the User Manual in the Supplement.



6 Conclusion

The existing spatial resolution of global LCC products is below 300 m, which increasingly fails to meet the growing demand
390 for more precise applications. This study produced the first global high-resolution LCC product (MuSyQ Global LCC) with a
spatial resolution of up to 10 m. The product was generated using Sentinel-2 data based on the empirical regression method of
the chlorophyll sensitive index (CSI) employed in producing MuSyQ LCC products across China. The high-resolution MuSyQ
product can exhibit more spatial detail features, benefiting precision agriculture and forestry applications more than the existing
products. The validation results indicate that the accuracy of the 10 m resolution MuSyQ Global LCC product is higher than
395 that of existing low-resolution products with an RMSE of 15.33 $\mu\text{g}/\text{cm}^2$ and R^2 of 0.27. When resampled to a 500 m resolution,
the MuSyQ Global LCC product demonstrates good consistency with the MODIS LCC product. Its accuracy (RMSE = 14.16
 $\mu\text{g}/\text{cm}^2$, bias = 1.68 $\mu\text{g}/\text{cm}^2$) is slightly higher than that of the MODIS product (RMSE = 14.74 $\mu\text{g}/\text{cm}^2$, bias = -2.65 $\mu\text{g}/\text{cm}^2$)
at NEON sites.

Author contribution

400 H. Z. designed the algorithm and wrote the original manuscript. J. L. and Q. L. organized the generation of the product. C. G.,
X. W. generated the product and L. G. developed the web interface. F. M. helped to revise the original manuscript. Y. D. and
J. Z. organized the experiments and S. L., W. Y. carried them out.

Competing interests

The authors declare that they have no conflict of interest.

405 Acknowledgments

This work was supported by the National Key Research and Development Program (2023YFB3907401) and the National
Natural Science Foundation of China (42271359).

References

410 Botha, E. J., Leblon, B., Zebarth, B., and Watmough, J.: Non-destructive estimation of potato leaf chlorophyll from canopy
hyperspectral reflectance using the inverted PROSAIL model, *International Journal of Applied Earth Observation and
Geoinformation*, 9, 360–374, <https://doi.org/10.1016/j.jag.2006.11.003>, 2007.



- Chen, J. M. and Leblanc, S. G.: A four-scale bidirectional reflectance model based on canopy architecture, *IEEE Transactions on Geoscience and Remote Sensing*, 35, 1316–1337, <https://doi.org/10.1109/36.628798>, 1997.
- 415 Croft, H., Chen, J. M., Wang, R., Mo, G., Luo, S., Luo, X., He, L., Gonsamo, A., Arabian, J., Zhang, Y., Simic-Milas, A., Noland, T. L., He, Y., Homolová, L., Malenovský, Z., Yi, Q., Beringer, J., Amiri, R., Hutley, L., Arellano, P., Stahl, C., and Bonal, D.: The global distribution of leaf chlorophyll content, *Remote Sensing of Environment*, 236, <https://doi.org/10.1016/j.rse.2019.111479>, 2020.
- 420 Feret, J.-B., François, C., Asner, G. P., Gitelson, A. A., Martin, R. E., Bidel, L. P. R., Ustin, S. L., Le Maire, G., and Jacquemoud, S.: PROSPECT-4 and 5: Advances in the leaf optical properties model separating photosynthetic pigments, *Remote Sensing of Environment*, 112, 3030–3043, <https://doi.org/10.1016/j.rse.2008.02.012>, 2008.
- Gitelson, A. A., Gritz †, Y., and Merzlyak, M. N.: Relationships between leaf chlorophyll content and spectral reflectance and algorithms for non-destructive chlorophyll assessment in higher plant leaves, *Journal of Plant Physiology*, 160, 271–282, <https://doi.org/10.1078/0176-1617-00887>, 2003.
- 425 Gu, C., Li, J., Liu, Q., Zhang, H., Liu, L., Mumtaz, F., Dong, Y., Zhao, J., Wang, X., and Liu, C.: Retrieving decametric-resolution leaf chlorophyll content from GF-6 WFV by assessing the applicability of red-edge vegetation indices, *Computers and Electronics in Agriculture*, 215, 108455, <https://doi.org/10.1016/j.compag.2023.108455>, 2023.
- Guan, L., Zhang, H., Li, J., Gu, C., Wang, Xiaohan, Xiao, X., Liu, Q., Zhou, Q., and Wu, W.: A dataset of 30 m/10-day spatio-temporal continuous leaf chlorophyll content of MuSyQ GF-series (2021–2022, China), , <https://doi.org/10.57760/sciencedb.16673>, 2025.
- 430 Jacquemoud, S., Verhoef, W., Baret, F., Bacour, C., Zarco-Tejada, P. J., Asner, G. P., François, C., and Ustin, S. L.: PROSPECT+SAIL models: A review of use for vegetation characterization, *Remote Sensing of Environment*, 113, S56–S66, <https://doi.org/10.1016/j.rse.2008.01.026>, 2009.
- Li, J., Zhang, H., Wang, X., Zhang, Z., Gu, C., Wen, Y., Chu, T., and Liu, Q.: MuSyQ 30m/10days leaf chlorophyll content product (from 2019 to 2020 across China version 01), , <https://doi.org/10.11922/sciencedb.j00001.00265>, 2021.
- 435 Lu, X., Croft, H., Chen, J. M., Luo, Y., and Ju, W.: Estimating photosynthetic capacity from optimized Rubisco–chlorophyll relationships among vegetation types and under global change, *Environ. Res. Lett.*, 17, 014028, <https://doi.org/10.1088/1748-9326/ac444d>, 2022.
- 440 Luo, X., Croft, H., Chen, J. M., Bartlett, P., Staebler, R., and Froelich, N.: Incorporating leaf chlorophyll content into a two-leaf terrestrial biosphere model for estimating carbon and water fluxes at a forest site, *Agricultural and Forest Meteorology*, 248, 156–168, <https://doi.org/10.1016/j.agrformet.2017.09.012>, 2018.
- Luo, X., Croft, H., Chen, J. M., He, L., and Keenan, T. F.: Improved estimates of global terrestrial photosynthesis using information on leaf chlorophyll content, *Global Change Biology*, 25, 2499–2514, <https://doi.org/10.1111/gcb.14624>, 2019.
- National Ecological Observatory Network (NEON): Plant foliar traits (DP1.10026.001), , <https://doi.org/10.48443/1E9E-E315>, 2024.
- 445 Qian, X., Liu, L., Chen, X., Zhang, X., Chen, S., and Sun, Q.: Global Leaf Chlorophyll Content Dataset (GLCC) from 2003–2012 to 2018–2020 Derived from MERIS and OLCI Satellite Data: Algorithm and Validation, *Remote Sensing*, 15, 700, <https://doi.org/10.3390/rs15030700>, 2023.



- 450 Schimel, D., Pavlick, R., Fisher, J. B., Asner, G. P., Saatchi, S., Townsend, P., Miller, C., Frankenberg, C., Hibbard, K., and Cox, P.: Observing terrestrial ecosystems and the carbon cycle from space, *Global Change Biology*, 21, 1762–1776, <https://doi.org/10.1111/gcb.12822>, 2015.
- Singh, P., Srivastava, P. K., Verrelst, J., Mall, R. K., Rivera, J. P., Dugesar, V., and Prasad, R.: High resolution retrieval of leaf chlorophyll content over Himalayan pine forest using Visible/IR sensors mounted on UAV and radiative transfer model, *Ecological Informatics*, 75, 102099, <https://doi.org/10.1016/j.ecoinf.2023.102099>, 2023.
- 455 van der Tol, C., Verhoef, W., Timmermans, J., Verhoef, A., and Su, Z.: An integrated model of soil-canopy spectral radiances, photosynthesis, fluorescence, temperature and energy balance, *Biogeosciences*, 6, 3109–3129, <https://doi.org/10.5194/bg-6-3109-2009>, 2009.
- Wang, X., Li, J., Zhang, H., Liu, Q., Liu, L., Gu, C., Mumtaz, F., Zhao, J., Dong, Y., Bai, J., Chu, T., Liu, C., Guan, L., and Huang, W.: Intercomparison and validation of five existing leaf chlorophyll content products over China, *International Journal of Applied Earth Observation and Geoinformation*, 130, 103930, <https://doi.org/10.1016/j.jag.2024.103930>, 2024.
- 460 Xu, M., Liu, R., Chen, J. M., Liu, Y., Shang, R., Ju, W., Wu, C., and Huang, W.: Retrieving leaf chlorophyll content using a matrix-based vegetation index combination approach, *Remote Sensing of Environment*, 224, 60–73, <https://doi.org/10.1016/j.rse.2019.01.039>, 2019.
- Xu, M., Liu, R., Chen, J. M., Liu, Y., Wolanin, A., Croft, H., He, L., Shang, R., Ju, W., and Zhang, Y.: A 21-year time series of global leaf chlorophyll content maps from MODIS imagery, *IEEE Transactions on Geoscience and Remote Sensing*, 60, 1–13, 2022a.
- 465 Xu, M., Liu, R., Chen, J. M., Shang, R., Liu, Y., Qi, L., Croft, H., Ju, W., Zhang, Y., and He, Y.: Retrieving global leaf chlorophyll content from MERIS data using a neural network method, *ISPRS Journal of Photogrammetry and Remote Sensing*, 192, 66–82, <https://doi.org/10.1016/j.isprsjprs.2022.08.003>, 2022b.
- Yang, F., Ren, H., Li, X., Hu, M., and Yang, Y.: Assessment of MODIS, MERIS, GEOV1 FPAR Products over Northern China with Ground Measured Data and by Analyzing Residential Effect in Mixed Pixel, *Remote Sensing*, 6, 5428–5451, <https://doi.org/10.3390/rs6065428>, 2014.
- 470 Yu, W., Li, J., Liu, Q., Zeng, Y., Zhao, J., Xu, B., and Yin, G.: Global Land Cover Heterogeneity Characteristics at Moderate Resolution for Mixed Pixel Modeling and Inversion, *Remote Sensing*, 10, 856, <https://doi.org/10.3390/rs10060856>, 2018.
- Zhang, H., Li, J., Liu, Q., Lin, S., Huete, A., Liu, L., Croft, H., Clevers, J. G. P. W., Zeng, Y., Wang, X., Gu, C., Zhang, Z., Zhao, J., Dong, Y., Mumtaz, F., and Yu, W.: A novel red-edge spectral index for retrieving the leaf chlorophyll content, *Methods in Ecology and Evolution*, 13, 2771–2787, <https://doi.org/10.1111/2041-210x.13994>, 2022.
- 475 Zhang, H., Li, J., Gu, C., Wang, X., Guan, L., and Liu, Q.: MuSyQ Global Leaf Chlorophyll Content product with 100m/10 days resolution(2019), , <https://doi.org/10.57760/sciencedb.19595>, 2025a.
- Zhang, H., Li, J., Gu, C., Wang, X., Guan, L., and Liu, Q.: MuSyQ Global Leaf Chlorophyll Content product with 100m/10 days resolution(2020), , <https://doi.org/10.57760/sciencedb.19687>, 2025b.
- 480 Zhang, H., Li, J., Gu, C., Wang, X., Guan, L., and Liu, Q.: MuSyQ Global Leaf Chlorophyll Content product with 100m/10 days resolution(2021), , <https://doi.org/10.57760/sciencedb.19689>, 2025c.
- Zhang, H., Li, J., Gu, C., Wang, X., Guan, L., and Liu, Q.: MuSyQ Global Leaf Chlorophyll Content product with 100m/10 days resolution(2022), , <https://doi.org/10.57760/sciencedb.19691>, 2025d.



485 Zhang, H., Li, J., Gu, C., Wang, X., Guan, L., and Liu, Q.: MuSyQ Global Leaf Chlorophyll Content product with 100m/10 days resolution(2023), , <https://doi.org/10.57760/sciencedb.19692>, 2025e.

Zhang, X., Liu, L., Chen, X., Gao, Y., Xie, S., and Mi, J.: GLC_FCS30: global land-cover product with fine classification system at 30 m using time-series Landsat imagery, *Earth System Science Data*, 13, 2753–2776, <https://doi.org/10.5194/essd-13-2753-2021>, 2021.

490